

Tracking Nanometer-Scale Fluorescent Particles in Two Dimensions With a Confocal Microscope

Zhaolong Shen, *Student Member, IEEE*, and Sean B. Andersson, *Member, IEEE*

Abstract—A system for tracking multiple nanometer-scale fluorescent particles in a confocal microscope and an experimental validation is described. Position estimates of an individual fluorescent particle are generated from fluorescence intensity measurements taken at a small number of discrete locations. Tracking is achieved by combining the estimation procedure with a linear quadratic Gaussian (LQG) regulator. Multiple particles are tracked by combining the models for individual particles into a single system, applying the same LQG framework, and then cycling the control through each subsystem in turn. Experimental results are presented for single and multiple particles. For validation purposes, during each experiment images from a charge-coupled device camera were captured and analyzed offline using a standard Gaussian fit method. The estimated trajectories were in good agreement with those produced by the LQG algorithm, thereby verifying the tracking scheme.

Index Terms—Fluorescence microscopy, linear-quadratic-gaussian (LQG) control, particle tracking.

I. INTRODUCTION

THE ability to image and analyze single molecules is a powerful tool in molecular biology that continues to be used to significantly advance knowledge of a wide-range of systems [1]. Example applications include the study of the nuclear trafficking process of influenza virus infection by tracking single vRNPs in living cells [2], and an exploration of the mechanisms leading to slow diffusion rates in cell membranes [3]. In addition, researchers have tracked multiple particles simultaneously, with applications including the measurement of heterogeneities in the microenvironment [4] and micromechanical properties [5]. Furthermore, such methods can even be used for drug and gene delivery [6]. Recent collections of review articles include [1], [7], and [8].

Most tracking methods rely on the use of a wide-field fluorescence image captured with a charge-coupled device (CCD) camera. Isolated point sources in the image can be localized with a precision far below the diffraction limit using a variety of means, such as centroid estimation [9], fitting of the image to a Gaussian profile [10], or other numerical schemes [11]. Recent advances in fluorescent dyes and in imaging techniques allow these localization methods to be used to generate super-resolution images even when the sources are not isolated [12]. These

methods in general are limited to tracking motion in or near the focal plane. Moreover, due to the need to collect a relatively large number of photons to assure good signal-to-noise ratio (SNR) [13], they are relatively limited in temporal resolution with respect to the time scale of the motion of single molecules. Methods for position estimation in three dimensions do exist, such as the use of defocusing [14], [15], the introduction of astigmatism [16], or tracking in scanning confocal microscopy [17]. These schemes, however, further reduce the temporal resolution.

To overcome such limitations, several alternative approaches have been developed to track a single nanometer-scale fluorescent particle. These schemes rely on point detectors in a single or multiphoton microscope. One early approach proposed rapidly steering the laser focus around a circle and estimating the particle position from collected fluorescence intensity fluctuations [18]. This basic scheme has been used in a variety of recent efforts. In [19], a feedback controller was introduced to steer the center of the scanned circle. To track in three dimensions, the focus was circularly scanned in two different axial planes in a sequential fashion [20], or a pair of laser beams were focused at different axial positions [21]. This latter scheme has been quite successful and has tracked quantum dots diffusing with coefficient as high as $20 \mu\text{m}^2/\text{s}$. Other tracking approaches include [22]–[24], which track particles moving in three dimensions without scanning the focus but at the expense of a more complicated detection system. Recent reviews of the state-of-the-art can be found in [1] and [25].

Our tracking system is composed of a confocal microscope with a piezoactuated nanopositioning stage, a microcontroller and a tracking algorithm based on the use of a linear quadratic Gaussian (LQG) controller. In this work, we use a position estimation algorithm introduced by one of the authors [26], [27], to estimate the particle position by taking measurements of the fluorescence intensity at several discrete locations. The overall implementation is simpler in terms of the experimental apparatus than existing methods and extends naturally to the tracking of multiple particles. Because the method is essentially algorithmic, application of the scheme to systems using beam steering instead of sample actuation and to those employing alternative sensing methods such as dual objective multifocal plane microscopy [28] is straightforward. It is also important to note that all tracking results reported to date for particles with diffusion coefficients above $0.1 \mu\text{m}^2/\text{s}$, including those presented here, utilize quantum dots. Consequently the signal-to-noise ratio (SNR) is high relative to what could be expected when using fluorescent dyes, particularly inside live cells. The estimation algorithm at the core of our method has been shown to be effective at low SNR [27] and thus we expect our algorithm to maintain performance in noisier settings.

Manuscript received January 19, 2010; revised May 06, 2010; accepted July 28, 2010. Manuscript received in final form August 10, 2010. Recommended by Associate Editor S. Matteo. This work was supported in part by the NSF through DBI-0649823 and CMMI-0845742.

The authors are with the Department of Mechanical Engineering, Boston University, Boston, MA 02215 USA (e-mail: zlshen@bu.edu; sanderss@bu.edu).

Color versions of one or more of the figures in this brief paper are available online at <http://ieeexplore.ieee.org>.

Digital Object Identifier 10.1109/TCST.2010.2067449

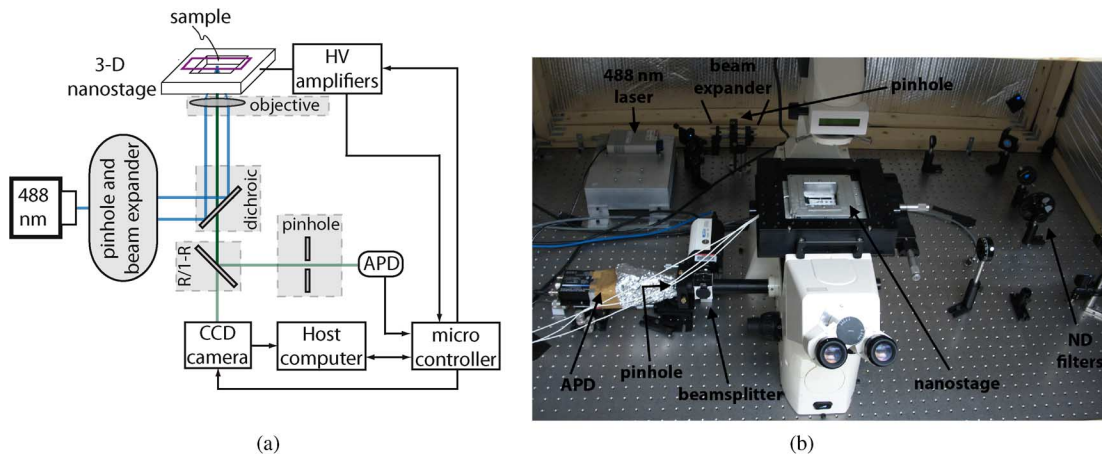


Fig. 1. Confocal tracking microscope. Fluorescence is excited in the sample using a laser beam focused to a diffraction-limited spot through the objective lens. Output fluorescence is collected by the objective and separated from the laser using a dichroic filter. This signal is passed through a beamsplitter, sending a fraction R to a CCD camera and $1-R$ to an APD. The tracking algorithm is implemented in a microcontroller. The CCD camera is used during initialization but is otherwise not part of the tracking algorithm. (a) Block diagram. (b) Physical apparatus.

The algorithm presented in this work previously appeared in [29] with preliminary experimental results in [30]. In this brief paper we describe a new physical implementation on a custom-built confocal microscope and a new and more detailed collection of tracking experiments. In particular, the system was augmented to allow the simultaneous capture of CCD images. Post-processing these images using the common Gaussian fit estimation procedure provided an independent measurement of the particle position in two dimensions and a verification of the tracking. It should be noted that splitting the output signal to achieve this lowers the overall SNR and would therefore not be done in practice, especially when applying the system to particles inside living cells where the SNR is inherently low.

This brief paper is organized as follows. In Section II, we describe the experimental apparatus. The position estimation and control algorithms are discussed in Section III, including the extension to multiple particles. Experimental results for tracking a fixed particle are described in Section IV, followed by those for tracking a single diffusing particle in Section V. Results for tracking multiple particles are described in Section VI and concluding remarks, including a discussion of limitations and our approach to overcoming them, are given in Section VII.

II. CONFOCAL TRACKING MICROSCOPE

We constructed a custom-designed confocal tracking microscope, shown in Fig. 1. A 488 nm laser (ChromaLASE, Blue Sky Research, CA) was spatially filtered using a $5 \mu\text{m}$ pinhole and expanded to fill the back aperture of the objective lens (water immersion, 63x, 1.2 N.A. C-Apochromat, Carl Zeiss, NY). The beam was directed into the objective lens using a dichromatic filter (T495LP, Chroma, VT). The resulting fluorescence was collected by the same objective lens, passed through the dichroic filter and then through a bandpass filter (HW625/30 m, Chroma, VT) to separate the excitation signal from the output. The output fluorescence was split into two beams using a beamsplitter. A fraction R (33%) was focused onto a CCD camera (Retiga EXi, QImaging, BC, Canada). The remaining signal was focused through a $25 \mu\text{m}$ pinhole

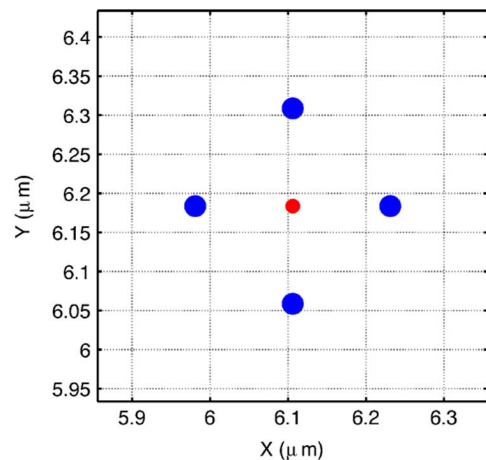


Fig. 2. In this work, we use a four-point measurement constellation. The measurement locations are equally spaced around a circle. It is the position of the center of this circle that is controlled using the LQG algorithm to track the position of the fluorescent molecule.

and onto the detector of an avalanche photodiode (APD) (SPCM-AQR-14, Perkin Elmer, MA).

In our setup, the focal point of the microscope is held fixed in space and the sample moved using a piezoelectric nanopositioning stage (Nano-PDQ, Mad City Labs, WI). The stage is a “frame-in-frame” style (see, e.g., [31]) with independent motion in the different directions, though with different dynamic characteristics. The stage is equipped with a sensing system with a manufacturer-reported accuracy on the order of picometers and is operated in a closed-loop mode in which the position is controlled to the user inputted-reference signal using a simple proportional-integral (PI) feedback controller designed by the manufacturer. We identified the dynamics of our stage in both the x - and y -directions using the step response of the stage. Using the identification toolbox in MATLAB to fit the response to a second-order system yielded the models

$$G_x = \frac{-88.8(s - 9030)}{s^2 + 2(0.66)(894)s + 894^2}$$

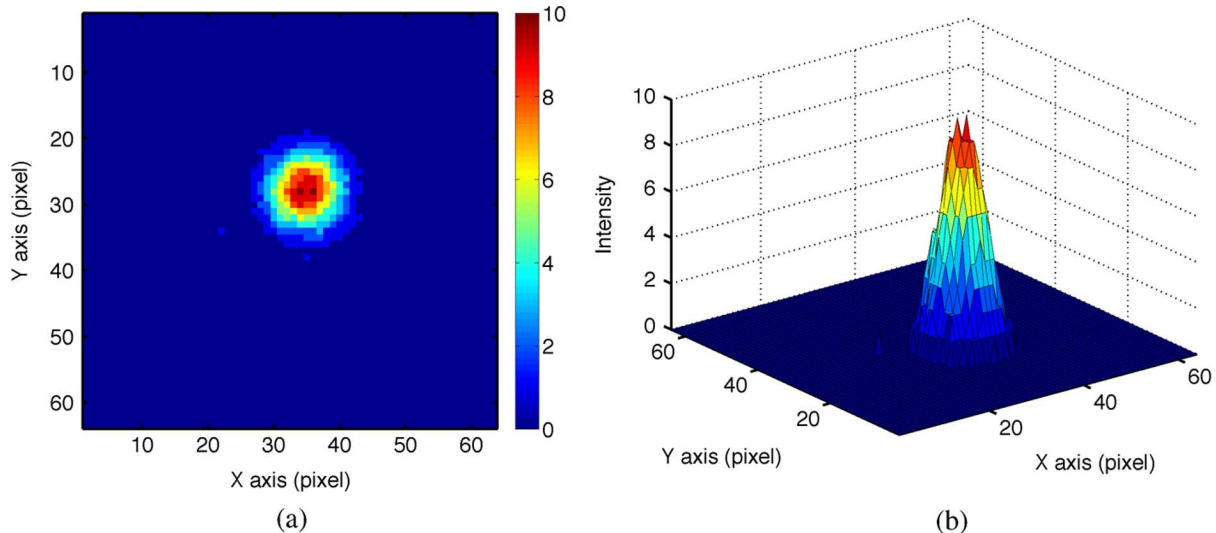


Fig. 3. Typical CCD image of a single quantum dot (or aggregation of dots—see text) in our system. The exposure time was 10 ms. (a) CCD image. (b) 3-D view.

$$G_y = \frac{-35.4(s - 4890)}{s^2 + 2(0.963)(416)s + 416^2}. \quad (1)$$

III. POSITION ESTIMATION AND CONTROLLER DESIGN

The tracking algorithm combines a standard LQG controller to drive the tracking error to zero with a scheme to convert a collection of intensity measurements into an estimate of the position of the fluorescent particle. Below we outline the steps in the algorithm. A full description of the position estimation scheme can be found in [27] while further details on the control approach can be found in [29].

A. Position Estimation

The need to accurately localize a fluorescent particle is common to all single particle tracking schemes. In optical microscopy, the output fluorescence from a point source, known as the point spread function (PSF) [32], limits the optical resolution to a few hundred nanometers. The position of the source particle, however, can be determined with sub-diffraction limit accuracy by determining the center of the PSF. One of the most common and accurate approaches to achieve this is to fit the measured intensity pattern to a Gaussian profile. With sufficiently high SNR, accuracy on the order of one nanometer can be achieved [33]. The method, however, relies on a large collection of measurements for an accurate fit of the model function. In the confocal setting, these measurements are acquired sequentially, leading to a severe restriction in the update rate of any controller depending on the estimate.

In our controller we use the fluoroBancroft algorithm developed by one of the authors [26], [27]. This algorithm yields an analytical solution to the position estimation problem from as few as three measurements taken at three non-collinear points. The algorithm has been shown to have an accuracy similar to Gaussian fitting in the wide-field setting [27]. The effect of the number of measurements used, as well as of the integration time of each measurement, has been explored in simulation in [29]

and [34]. In general, for a fixed particle, increasing the integration time or the number of measurements improves the estimation precision. For a diffusing particle, however, motion occurs throughout the measurement process. This unmodeled motion leads to increased error in the estimation. At high SNR, as in the current work, even four measurements are sufficient for tracking. Increasing the number of measurements or the integration time of each measurement can help to overcome the challenge of tracking in systems with lower SNR at the cost of reducing the maximum diffusion coefficient which can be accurately tracked.

In the work described in this brief paper, we obtain four intensity measurements as follows. For each actuator command generated by the tracking controller (cf. Section III-B), the focal point is moved through four points lying on a circle centered on the commanded position (see Fig. 2). At each point, the stage is given a small amount of time to settle and then photon counts are collected from the APD for a fixed integration time T_{int} .

B. Controller Design

Because the cross-axis coupling of the stage is negligible, we assume motion in the two lateral directions is independent. Consider first motion in the x -direction. The Brownian motion of a particle in one dimension is described by the stochastic differential equation

$$dx_p(t) = \sqrt{2D}dw_x(t) \quad (2)$$

where x_p is the position of particle, D is its diffusion coefficient, and $dw_x(t)$ is an infinitesimal Wiener increment with mean 0 and variance dt , the sampling time of the system. The dynamics of the stage are given by a second-order transfer function model of the form in (1). We define the state of the system in this one direction to be

$$X_x = [x_p \ x_s \ \dot{x}_s \ u_x]^T \quad (3)$$

where x_s is the position of the stage. Due to the zero in the transfer function, we include the command voltage u_x in the

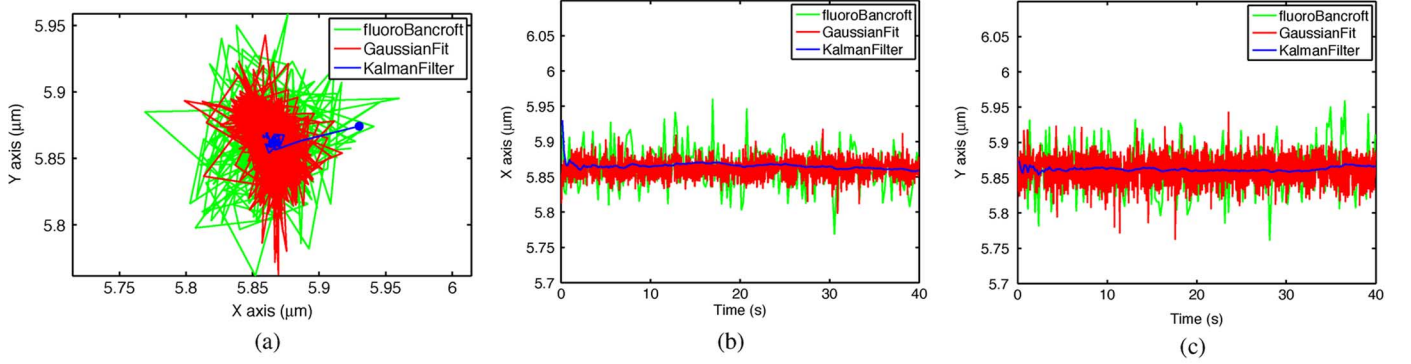


Fig. 4. Tracking run with a fixed particle. The center line (blue) is the output of the Kalman filter, the noisiest line (green) are the raw estimates determined by the fluoroBancroft algorithm, and the intermediate line (red) are the Gaussian fit estimates. The standard deviation in the position estimates from the algorithm (output of the Kalman filter) were (2.9, 2.6) nm in (x, y) . The standard deviation in the raw estimates from the fluoroBancroft algorithm were (31.0, 36.8) nm while the estimates based on the Gaussian fit had a standard deviation of (15.4, 23.2) nm. (a) Planar trajectory. (b) Trajectory in x . (c) Trajectory in y .

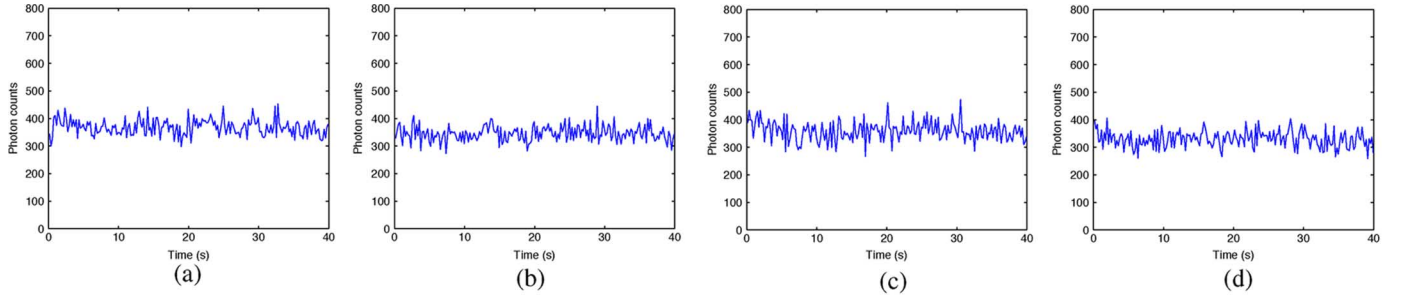


Fig. 5. Fluorescence readings for each of the four measurements locations during the tracking run in Fig. 4. The integration time was 2 ms. (a) Right position. (b) Top position. (c) Left position. (d) Bottom position.

system state and view the first time-derivative of this driving signal as the control for purposes of developing the LQG controller. The value of u_x is then extracted from the state at every step and applied to the system.

For the observations, we assume we have a measurement of the particle position x_p (obtained using the fluoroBancroft algorithm described in Section III-A). The position of the stage is measured from the stage sensors. We model the system output as the difference between these two signals plus measurement noise

$$y_x(t) = x_p(t) - x_s(t) + v_x(t). \quad (4)$$

The primary source of noise in our system is shot noise in the intensity measurement with additional noise coming from the background intensity, electronic noise in the APD, and noise in the stage sensors. These noise sources are filtered through the fluoroBancroft estimator to generate v_x . For the purposes of the system model, we assume the measurement noise has a known covariance, determined through experiment, given by

$$V_x = E[v_x v_x^T] \quad (5)$$

where $E[\cdot]$ represents the expected value.

The linear stochastic dynamic system for the x -axis in state space form is then given by

$$\dot{X}_x = A_x X_x + B_x U_x + W_x, \quad Y_x = C_x X_x + v_x \quad (6)$$

where the state-space matrices are derived from the stage transfer function in (1) and from the particle dynamics in (2). To represent the Brownian motion of the particle, we take the covariance of $W_x(t)$ to be

$$\Sigma_{W_x} = E[W_x W_x^T] = \text{diag}(2Ddt, 0, 0, 0) \quad (7)$$

where $\text{diag}(\cdot)$ represents a diagonal matrix.

The y -axis can be modeled in the same manner as the x -axis, though with different dynamics. The system model for tracking a single particle in two dimensions is then given by appending the y -axis model to that of the x -axis. This continuous model is discretized for a given controller update period dt . We then apply a standard discrete-time LQG controller (see, e.g., [35]) with a cost function given by

$$J = \sum_{k=1}^{\infty} [\lambda_x (x_p(k) - x_s(k))^2 + \lambda_y (y_p(k) - y_s(k))^2 + \lambda_u (u_x^2 + u_y^2)] \quad (8)$$

where λ_x and λ_y are the weights for the state and λ_u is the weight for the control.

The control scheme for tracking a single particle is then as follows. Denote the current state estimate generated by the Kalman filter in the LQG controller as \hat{X} . The nominal command voltage of the stage (\hat{u}_x, \hat{u}_y) is extracted from the estimate. Based on

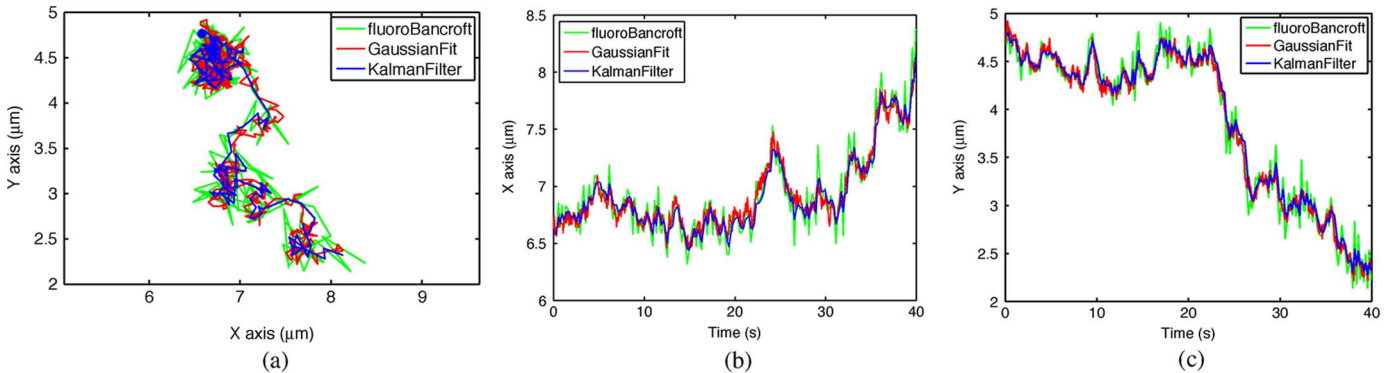


Fig. 6. Tracking run with a diffusing particle with a relatively small D . As with the fixed particle results in Fig. 4, the raw fluoroBancroft estimates show the largest variance while the filtered estimates show the least. (a) Planar trajectory. (b) Trajectory in x . (c) Trajectory in y .

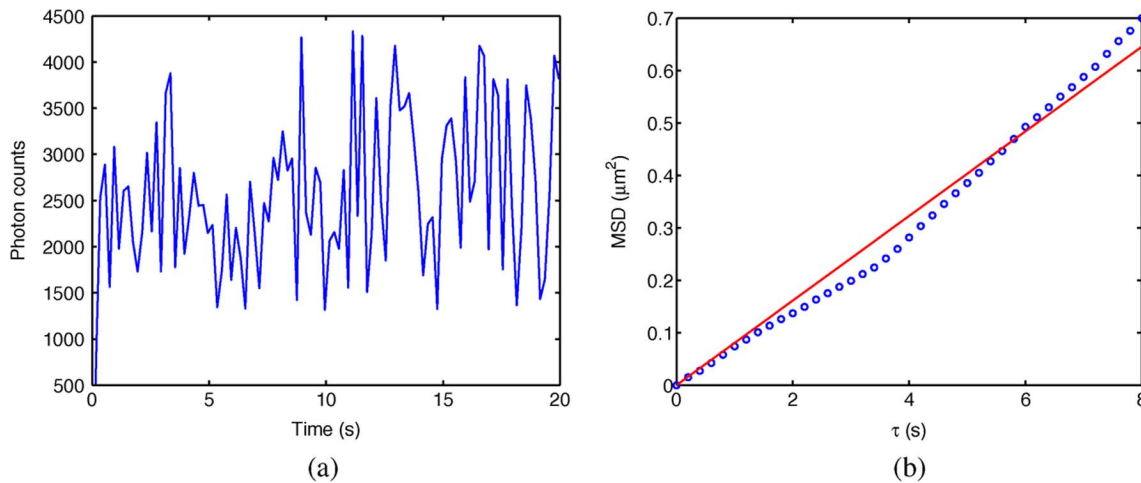


Fig. 7. Results from tracking a slowly diffusing particle. (a) Fluorescence intensity at the right-most measurement location during the tracking run in Fig. 6. Rapid variations reflect the shot noise while slower variations reflect the diffusion of the particle in the axial direction. (b) The MSD values (open circles) were fitted to a curve of the form (9) (fitted curve shown as red solid line) to produce an estimate of $D = 0.020 \mu\text{m}^2/\text{s}$. (a) Measured fluorescence intensity. (b) MSD plot.

these values, the stage is moved according to the scan procedure described in Section III-A and the particle position estimated using the fluoroBancroft algorithm. The state measurement is calculated using (4) and this measurement is fed to the LQG controller to update the state estimate. The process is then repeated.

To track N particles, we independently define a state-space model for each particle and an LQG controller for each. As there is only one translation stage, we simply cycle through each system in turn. As a result, the controller rate is N times longer than in the single particle case. Optimizing both the cycle sequence and the relative amount of time spent on each particle remains an open problem.

When tracking multiple particles, we assume they are well separated so that their PSFs do not overlap. (For comments on approaching the problem when this assumption fails, see Section VI.) As a result, one of the primary differences between single and multiple particle tracking is the need for a relatively large shift in the actuators when moving between particles. Due to the actuator dynamics and depending on the sampling time of the system, overshoot or other transient effects may lead to poor positioning of the focal volume of the microscope. In extreme cases, this error may be large enough that the particle is not in-

side the focal volume at all, leading to loss of tracking. It is therefore important to design low-level controllers that yield small one-step positioning errors to improve tracking performance in the multiple particle case.

IV. TRACKING A FIXED PARTICLE

We implemented the tracking scheme of Section III on the apparatus described in Section II. We initially tested the algorithm on fixed quantum dots. These samples were prepared by diluting a solution of quantum dots (QD625, Invitrogen, USA) in glycerol. A small amount of this dilution was placed on a glass slide and sealed with a cover slip. The slide was mounted on the microscope and visually searched to find a quantum dot that had adsorbed onto the coverslip. Individual quantum dots in these experiments may actually have been aggregations of a small number of dots. So long as the entire aggregation was smaller than the diffraction limit, the resulting shape of the intensity function remained the same, though with a higher intensity. A typical CCD image of a fixed dot is shown in Fig. 3 together with a 3-D representation highlighting the shape of the PSF. The exposure time was 10 ms.

The update rate for the position of the stage, and thus the motion around the sampling point constellation shown in Fig. 2,

was set to 20 Hz. Since four measurement points were used, the update rate for the LQG controller was 5 Hz. The integration time at each measurement location was set to 2 ms while the radius of the circle was set to 125 nm. These values were chosen through trial and error. The radius represents the commanded value. Due to the dynamics of the stage the actual position of the focal point varied somewhat. The system recorded the stage position during the measurements and used these measurements, not the commanded values, during the position estimation process. The background noise rate, estimated by collecting data from a blank sample, was set to 1 count/ms. To determine the value of w_o , the width of the PSF, a Gaussian fit to a CCD image of a quantum dot (11×11 pixels) was performed, leading to a value of $w_o = 250$ nm. Based on prior experience with the fluoroBancroft position estimation algorithm, the covariance of the noise in the position estimate was set to $0.01 \mu\text{m}^2$ in each direction. The weights for the LQR cost function were set to $\lambda_x = \lambda_y = 1 \times 10^{40}$ and $\lambda_u = 1 \times 10^{-40}$, reflecting that since the control in the LQG algorithm is the derivative of the piezostage input, it is essentially unrestricted. The actual stage driving voltage was determined from the corresponding component of the predicted system state. Since setting the value of the diffusion coefficient D in the algorithm to $0 \mu\text{m}^2/\text{s}$ would lead to very slow convergence in the LQG, any initial error introduced by the user when selecting the initial conditions would persist for a long time. We therefore set D to a small but nonzero value ($1 \times 10^{-5} \mu\text{m}^2/\text{s}$). The tracking time was arbitrarily set to 40 s.

During a tracking run, we captured, at each of the four measurement locations, a CCD image with an integration time of 10 ms. A Gaussian fit was run off line on each of these images and the estimated position shifted according to the measured stage location to produce an estimate in a lab-fixed frame. This measurement is itself noisy with an accuracy similar to that of the fluoroBancroft algorithm (see, e.g., [10], [27], and results below). As a result, it does not provide a ground truth for the position of the quantum dot. It does, however, provide an independent measurement of the particle position and serves to verify the tracking procedure.

The results of a typical run are shown in Fig. 4, including the trajectory as determined by the output of the Kalman filter (center line, blue), the raw position estimates of the fluoroBancroft algorithm (noisiest line, green), and the results of the Gaussian fitting procedure (intermediate line, red). The steady-state standard deviation in the (x, y) position estimates over this run were (2.93, 2.60) nm for the optimal estimate provided by the Kalman filter, (31.0, 36.8) nm for the fluoroBancroft estimates, and (15.4, 23.2) nm for the Gaussian fit estimates. Both unfiltered measurements were significantly below the Rayleigh diffraction limit of approximately 317 nm for our optical setup. As expected, the filtered estimates were much more accurate. Note that the initial condition was provided through a user click based on the CCD image and included a much larger initial error in x than in y . Note also that the fluoroBancroft estimates are only slightly less precise than the Gaussian fit estimates despite the fact that only four measurements were used in the former while 121 measurements from the 11×11 pixel array were used in the latter. It is difficult, however, to draw any conclusions regarding

the performance of the two algorithms since the signal levels are not similar due to an uneven split of the output intensity between the CCD and the avalanche photodiode and because the integration times are different. A detailed comparison was performed in [27].

The measured intensities at each of the four measurement locations during the run in Fig. 4 are shown in Fig. 5. The average values were just under 400 counts for each location. Since the measurement locations were designed to be equally distant from the center of the source, the signals should have the same mean value. The top and bottom measurement positions have slightly lower means, reflecting either a small asymmetry in the actual point spread function or an effect of the different dynamics of the stage in the two directions.

V. TRACKING SINGLE DIFFUSING PARTICLES

To apply our algorithm to diffusing particles, we prepared different dilutions of quantum dots in glycerol and water. Varying the proportion of water allowed us to vary the viscosity and thus the diffusion coefficients. All controller parameters other than the value of D and the integration time on the measurement were kept the same as for the experiments with the fixed quantum dot. The true theoretical value of D was not known exactly for two main reasons. First, the viscosity and experiment temperature were not carefully controlled. Second, our preparation seemed to lead to aggregations of a small number of quantum dots rather than to single dots. Since the size of these aggregations were still well below the diffraction limit, they appeared optically as a single dot (though with a brighter intensity) but with a smaller diffusion coefficient that depended on the number of dots in the aggregation. The integration time was set to 5 ms through trial and error.

After each experiment, we used the particle trajectory to calculate the mean squared displacement (MSD) according to

$$\begin{aligned} \text{MSD}(\tau) &= \langle (\hat{x}_p(t) - \hat{x}_p(t + \tau))^2 + (\hat{y}_p(t) - \hat{y}_p(t + \tau))^2 \rangle \\ &= 4D\tau \end{aligned} \quad (9)$$

where (\hat{x}_p, \hat{y}_p) is the estimated particle position from the Kalman filter and $\langle \cdot \rangle$ represents an ensemble average over the tracking run. The 2-D diffusion coefficient can be estimated from the slope of a linear fit to the MSD data. It should be noted that this approach assumes that the diffusion coefficient is constant throughout the tracking run. Furthermore, the estimate is valid only for values of τ larger than the dynamics of the tracking controller (on the order of the controller update rate). As a result, the estimate serves as a rough measure of the diffusion coefficient, allowing us to characterize the relative diffusion rates between runs. For details on estimating diffusion coefficients, see [36] and [38].

A. Sample Run With Slow Diffusion

The results of a typical tracking run for a slowly moving particle is shown in Figs. 6–7(b). For this run the integration time was increased from 2 to 5 ms to compensate for the lower intensities due to diffusion out of the image plane. The trajectory in

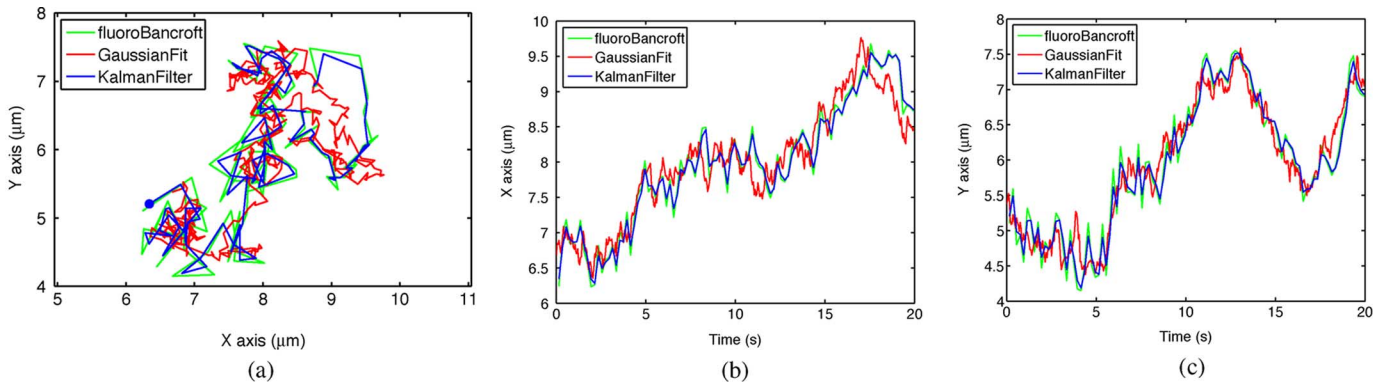


Fig. 8. Tracking run with a diffusing particle with a relatively large D . (a) Planar trajectory. (b) Trajectory in x . (c) Trajectory in y .

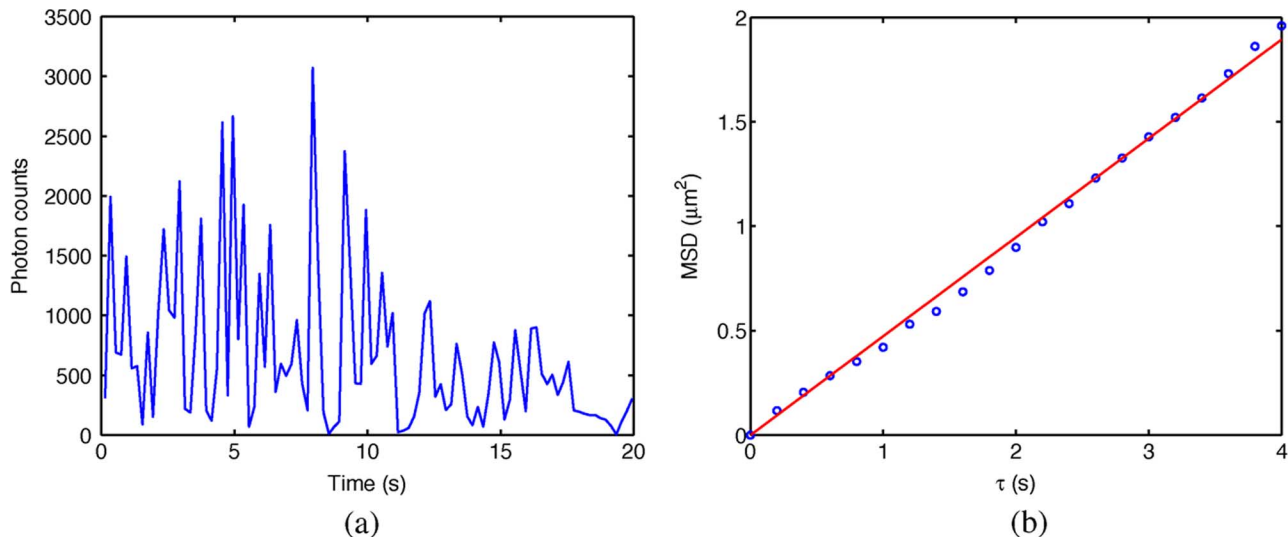


Fig. 9. Results from tracking a faster diffusing particle. (a) Fluorescence intensity at the right-most measurement location during the tracking run in Fig. 8. Rapid variations reflect shot noise while slower variations reflect diffusion of the particle in the axial direction. Variations are faster than in Fig. 7(a), reflecting the higher diffusion coefficient. (b) MSD values (open circles) and linear fit (solid line) yielding $D = 0.12 \mu\text{m}^2/\text{s}$. (a) Measured fluorescence intensity. (b) MSD plot.

Fig. 6 again shows the estimated trajectory, the raw fluoroBancroft estimates, and the Gaussian fitting estimates. As expected, the filtered estimates exhibited a smaller variation.

The fluorescence intensity from measurement position 1 (see Fig. 2) is shown in Fig. 7(a). The measurements from the other three positions were qualitatively similar. The average intensity, approximately 2200 photon counts, was significantly higher than for the fixed particle case in Fig. 5. This is partially explained by the increased integration time (from 2 to 5 ms). The average count is perhaps better expressed as approximately 440 counts/ms while in the fixed case it was 200 counts/ms. The additional increase is likely due a larger number of quantum dots in the aggregation being tracked. The trace also shows a significantly larger variance than in the fixed particle case, caused by two effects. First, because the particle was diffusing, there was more variation in the relative planar position of the particle and the position of the focal point of the microscope. Second, the particle was freely diffusing in three dimensions while tracking was being performed only in the focal plane.

The MSD for the run shown in Fig. 6 was calculated using (9) with the results shown in Fig. 7(b). Fitting this data with the form in (9) yielded $D = 0.020 \mu\text{m}^2/\text{s}$. The knee in the MSD values

likely reflects a change in diffusion coefficient during the run. This could arise from a variety of sources, including changes in the local viscosity. While not explored here, such changes can be important indicators into underlying processes (see, e.g., [2]).

B. Sample Run With Faster Diffusion

The results of a typical tracking run for a faster moving particle are shown in Figs. 8 and 9. Since with the larger diffusion coefficient the particle was more likely to diffuse away along the (untracked) optical axis, the tracking time was reduced to 20 s. The trajectory in Fig. 8 is similar in terms of the estimated values as with the fixed (see Fig. 4) and slowly diffusing particle cases (see Fig. 6). The measured fluorescence intensity from position 1 is shown in Fig. 9(a). The signal showed increased variability due to the higher diffusion coefficient. At times, the signal level approached zero, indicating near loss of tracking. The MSD, shown in Fig. 9(b), yielded $D = 0.12 \mu\text{m}^2/\text{s}$.

In experiments with even higher diffusion coefficients, loss of tracking was common. It should be noted, however, that the particle almost invariably diffused away along the untracked optical axis; planar tracking remained successful so long as there was

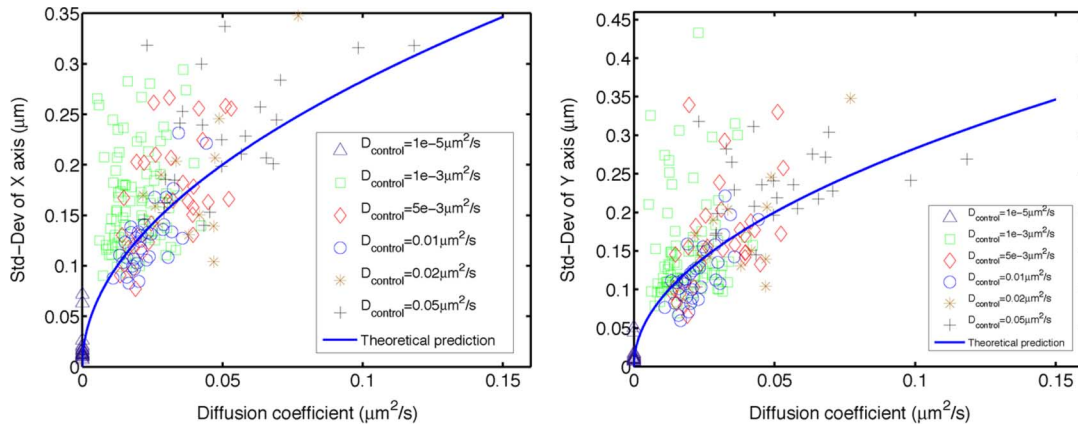


Fig. 10. Tracking error and theoretical error based on particle diffusion. The actual error is driven by diffusion, estimation error and mismatch of model parameters. Experiments with a chosen value of D closer to the estimated D were closer to the theoretical curve.

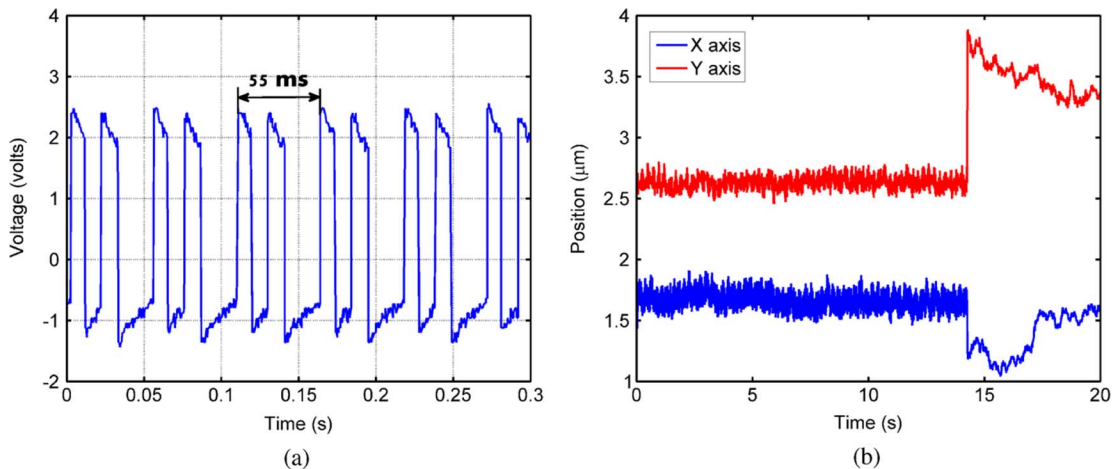


Fig. 11. Tracking at controller rate of 20 Hz. (a) Timing pattern. Each edge corresponds to a measurement position. (b) Trajectories calculated from Gaussian fitting on a sequence of CCD images. The images were not synchronized to the controller and trajectories reflect motion of the stage around the 125 nm-radius measurement constellation. The slower bandwidth of the y -axis resulted in a smaller motion in that direction, reflected in the smaller variance of the y -signal. At 14 s, the controller was turned off. The immediate jump was due to the stage resetting to its zero position. Residual motion reflects the untracked diffusion of the particle. (a) Timing. (b) Estimated trajectories.

a sufficiently high intensity. As discussed in Section VII, extension of the tracking algorithm to three dimensions requires a 3-D position estimation algorithm. While we have proposed such an extension of the fluoroBancroft algorithm in [26], experimental verification of the estimator is ongoing.

C. Tracking Performance

Because the true trajectory of the particle is unknown, the tracking error for a diffusing particle cannot be calculated exactly. It can, however, be approximately determined as follows. As described in Section IV, at every time step of a tracking run, a CCD image was captured at each of the four measurement points in the constellation. Under perfect tracking and position estimation, the position of the quantum dot would remain fixed in the sequence of images. Calculating the standard deviation of the position estimates determined by Gaussian fitting thus provides a measurement of the overall tracking error. This error is driven by a variety of factors with the most dominant being the diffusion of the particle during the measurement and control sequence. As seen in (2), the error in each axis should theoretically

grow as $\sqrt{2D dt}$ where dt is the control update time. The error is also affected, however, by estimation error in the Gaussian fitting, itself arising primarily from the shot noise in the photon measurements, as well as the mismatch between the diffusion coefficient used in the model and the true value.

A large number of tracking experiments were run on different particles. For each the diffusion coefficient was estimated from the MSD and a Gaussian fit was performed on each image taken at measurement location one. The resulting standard deviations in the x and y estimates as a function of estimated diffusion coefficient are shown in Fig. 10. Also shown is the theoretical curve given by $\sqrt{2D dt}$ where the value of dt was set to the update rate of 200 ms. The error generally increased with increasing diffusion coefficient. The measured error includes not only diffusion but also estimation error and model mismatch, leading to a generally larger error than the theoretical calculation predicts. In general, the farther the value chosen for D in the controller was from the diffusion coefficient estimated from the MSD calculation, the larger the error was, reflecting the effect of the mismatch.

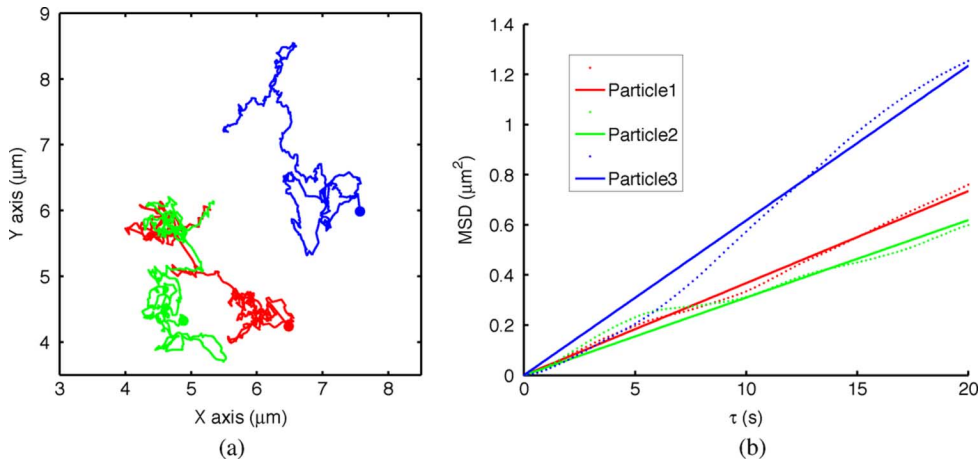


Fig. 12. Simultaneous tracking of three particles and corresponding MSD values (dotted lines) and linear fits (solid lines). The estimated values of D were $0.0092 \mu\text{m}^2/\text{s}$ (red), $0.0077 \mu\text{m}^2/\text{s}$ (green), and $0.015 \mu\text{m}^2/\text{s}$ (blue). At one point, two of the particles (green and red) moved close enough to become indistinguishable. The corresponding controller states converged with residual error between the trajectories due primarily to estimation error. The controller cannot detect a separation of one particle into two and thus tracked only one for the remainder of the run. (a) Estimated trajectories. (b) MSD.

D. Tracking At Higher Loop Rates

All experiments shown above were performed with an update rate for the LQG controller set to 5 Hz. This relatively slow rate was driven primarily by the communication constraints of the control hardware. Due to limited on-board storage of the microcontroller, the data acquired at each measurement location (photon counts, stage position, and CCD image) needed to be transmitted to the host system at every cycle of the control loop. Sending such information was required in order to verify and quantify tracking but is not required for tracking. To illustrate tracking at higher loop rates, we performed runs without sending any data back to the host system. Motion between the measurements was set to 100 Hz. As illustrated in Fig. 11(a), a digital I/O pin on the microcontroller was toggled prior to each measurement of the stage position. The delay after the fourth edge reflects the time for computation. In these runs, the LQG update rate was approximately 20 Hz. To illustrate tracking, images were captured simultaneously from the CCD using the host computer and Gaussian fitting used to estimate the trajectory. These images, however, were not synchronized to the control loop and thus could not be registered to each individual measurement constellation location. The variance in the estimates thus reflect not only shot noise and the motion of the particle during the integration time when capturing the CCD image, but also the motion of the stage around the measurement constellation during the acquisition time. As shown in Fig. 11(b), the particle was held approximately fixed relative to the image frame. At 14 s the controller was turned off. After an initial jump in the position as the stage reset to its zero position, the particle diffused freely, illustrating that the fixed position in the images was due to the tracking controller.

Note that tracking speed in the current system is limited primarily by the computational hardware and not fundamental limits due to shot noise (see, e.g., [37]–[39] for theoretical and experimental results of such limits).

VI. EXTENDING TO MULTIPLE PARTICLES

As discussed in Section III, the basic scheme can be extended to multiple particles by expanding the system state and then cycling through the particles during each control period. We implemented this scheme and applied it to freely diffusing quantum dots. The results of a typical run involving three particles is shown in Fig. 12(a). The MSDs for each of the three tracked particles are shown in Fig. 12(b). The resulting diffusion coefficients were calculated to be $0.0092 \mu\text{m}^2/\text{s}$ (red), $0.0077 \mu\text{m}^2/\text{s}$ (green), and $0.015 \mu\text{m}^2/\text{s}$ (blue). Due to the low diffusion coefficients, free diffusion along the optical axis was much lower. As a result, the tracking time was set to 300 s.

Our controller assumed that the particles were well-separated in space. During the tracking run shown, however, two of the particles came close enough together that their PSFs became indistinguishable. The position measurements were then the same up to measurement noise, and the two estimated trajectories essentially converged. The controller does not model such events and in general, if this occurs, will from that point on only follow one of the particles even if they separate. In order to follow multiple, interacting particles, one can turn to fluorescent labels whose emission spectra do not overlap, allowing the signals to be spectrally separated from each other.

VII. CONCLUSION AND FUTURE WORK

In this brief paper, we presented a scheme for tracking nanometer-size fluorescent particles that combines a position estimation algorithm with an LQG controller. We have validated the tracking capability in two dimensions through experiment. Our results indicate that the primary limitation of the scheme is the lack of 3-D capability. The extension of the LQG controller into 3-D is straightforward and we have proposed a modification of the fluoroBancroft algorithm for localization in three dimensions [26]. The method utilizes a 3-D version of the Gaussian model for the fluorescence intensity. While effective in deconvolution wide-field microscopy [40], other models have been proposed for two-photon microscopy [41] and the accuracy of our modeling in the confocal setting needs to be

theoretically analyzed and experimentally studied. We expect, however, that the feedback nature of the tracking process will help overcome challenges in the position estimation and that 3-D tracking will be readily achieved.

One of the primary limitations of our system when tracking multiple particles is the speed of the hardware and its ability to rapidly and accurately move the large distances between particles. Our implementation utilizes the closed-loop controller provided by the manufacturer of the nanopositioning stage. The bandwidth can be increased significantly by using more advanced controllers for the piezos such as tuned-PID [42] and robust controllers [43].

REFERENCES

- [1] W. E. Moerner, "New directions in single-molecule imaging and analysis," in *Proc. Nat. Acad. Sci.*, Jul. 2007, vol. 104, pp. 12-596-12-602.
- [2] H. P. Babcock, C. Chen, and X. Zhuang, "Using single-particle tracking to study nuclear trafficking of viral genes," *Biophys. J.*, vol. 87, no. 4, pp. 2749-2758, Oct. 2004.
- [3] K. Murase, T. Fujiwara, Y. Umemura, K. Suzuki, R. Iino, H. Yamashita, M. Saito, H. Murakoshi, K. Ritchie, and A. Kusumi, "Ultrafine membrane compartments for molecular diffusion as revealed by single molecule techniques," *Biophys. J.*, vol. 86, no. 6, pp. 4075-4093, Jun. 2004.
- [4] M. T. Valentine, P. D. Kaplan, D. Thota, J. C. Crocker, T. Gisler, R. K. Prud'homme, M. Beck, and D. A. Weitz, "Investigating the microenvironments of inhomogeneous soft materials with multiple particle tracking," *Phys. Rev. E*, vol. 64, pp. 061506-1-061506-9, 2001.
- [5] Y. Tseng, T. P. Kole, and D. Wirtz, "Micromechanical mapping of live cells by multiple-particle-tracking microrheology," *Biophys. J.*, vol. 83, pp. 3162-3176, 2002.
- [6] J. Suh, M. Dawson, and J. Hanes, "Real-time multiple-particle tracking: Applications to drug and gene delivery," *Adv. Drug Del. Rev.*, vol. 57, no. 1, pp. 63-78, Jan. 2005.
- [7] E. J. G. Peterman, H. Sosa, and W. E. Moerner, "Single-molecule fluorescence spectroscopy and microscopy of biomolecular motors," *Ann. Rev. Phys. Chem.*, vol. 55, pp. 79-96, 2004.
- [8] E. S. Yeung, "Dynamics of single biomolecules in free solution," *Ann. Rev. Phys. Chem.*, vol. 55, pp. 97-126, 2004.
- [9] M. K. Cheezum, W. F. Walker, and W. H. Guilford, "Quantitative comparison of algorithms for tracking single fluorescent particles," *Biophys. J.*, vol. 81, no. 4, pp. 2378-2388, Oct. 2001.
- [10] R. E. Thompson, D. R. Larson, and W. W. Webb, "Precise nanometer localization analysis for individual fluorescent probes," *Biophys. J.*, vol. 82, no. 5, pp. 2775-2783, May 2002.
- [11] A. J. Berglund, M. D. McMahon, J. J. McClelland, and J. A. Liddle, "Fast, bias-free algorithm for tracking single particles with variable size and shape," *Opt. Expr.*, vol. 16, no. 18, pp. 14-064-14-075, Sep. 2008.
- [12] S. W. Hell, "Far-field optical nanoscopy," *Science*, vol. 316, no. 5828, pp. 1153-1158, May 2007.
- [13] X. Michalet, S. Weiss, and M. Jäger, "Single-molecule fluorescence studies of protein folding and conformational dynamics," *Chem. Rev.*, vol. 106, no. 5, pp. 1785-1813, Apr. 2006.
- [14] H. P. Kao and A. S. Verkman, "Tracking of single fluorescent particles in three dimensions: Use of cylindrical optics to encode particle position," *Biophys. J.*, vol. 67, no. 3, pp. 1291-1300, Sep. 1994.
- [15] M. Speidel, A. Jonáš, and E.-L. Florin, "Three-dimensional tracking of fluorescent nanoparticles with subnanometer precision by use of off-focus imaging," *Opt. Lett.*, vol. 28, no. 2, pp. 69-71, 2003.
- [16] B. Huang, W. Wang, M. Bates, and X. Zhuang, "Three-dimensional super-resolution imaging by stochastic optical reconstruction microscopy," *Science*, vol. 319, no. 5864, pp. 810-813, Jan. 2008.
- [17] P. J. Lu, P. A. Sims, H. Oki, J. B. Macarthur, and D. A. Weitz, "Target-locking acquisition with real-time confocal (TARC) microscopy," *Opt. Expr.*, vol. 15, no. 14, pp. 8702-8712, Jul. 2007.
- [18] J. Enderlein, "Tracking of fluorescent molecules diffusing within membranes," *Appl. Phys. B*, vol. 71, no. 5, pp. 773-777, Nov. 2000.
- [19] A. J. Berglund and H. Mabuchi, "Feedback controller design for tracking a single fluorescent molecule," *Appl. Phys. B*, vol. 78, no. 5, pp. 653-659, Mar. 2004.
- [20] V. Levi, Q. Ruan, and E. Gratton, "3-D particle tracking in a two-photon microscope: Application to the study of molecular dynamics in cells," *Biophys. J.*, vol. 88, no. 4, pp. 2919-2928, Apr. 2005.
- [21] K. McHale, A. J. Berglund, and H. Mabuchi, "Quantum dot photon statistics measured by three-dimensional particle tracking," *Nano Lett.*, vol. 7, no. 11, pp. 3535-3539, Nov. 2007.
- [22] H. Cang, C. M. Wong, C. S. Xu, A. H. Rizvi, and H. Yang, "Confocal three dimensional tracking of a single nanoparticle with concurrent spectroscopic readouts," *Appl. Phys. Lett.*, vol. 88, no. 22, pp. 223901-1-223901-3, May 2006.
- [23] H. Cang, C. S. Xu, D. Montiel, and H. Yang, "Guiding a confocal microscope by single fluorescent nanoparticles," *Opt. Lett.*, vol. 32, no. 18, pp. 2729-2731, Sep. 2007.
- [24] G. A. Lessard, P. M. Goodwin, and J. H. Werner, "Three-dimensional tracking of individual quantum dots," *Appl. Phys. Lett.*, vol. 91, no. 22, p. 224106, Nov. 2007.
- [25] H. Cang, C. S. Xu, and H. Yang, "Progress in single-molecule tracking spectroscopy," *Chem. Phys. Lett.*, vol. 457, no. 4-6, pp. 285-291, May 2008.
- [26] S. B. Andersson, "Position estimation of fluorescent probes in a confocal microscope," in *Proc. IEEE Conf. Decision Control*, 2007, pp. 4950-4955.
- [27] S. B. Andersson, "Localization of a fluorescent source without numerical fitting," *Opt. Expr.*, vol. 16, no. 23, pp. 18-714-18-724, Nov. 2008.
- [28] S. Ram, P. Prabhat, E. S. Ward, and R. J. Ober, "Improved single particle localization accuracy with dual objective multifocal plane microscopy," *Opt. Expr.*, vol. 17, no. 8, pp. 6881-6898, Apr. 2009.
- [29] Z. Shen and S. B. Andersson, "LQG-based tracking of multiple fluorescent particles in two-dimensions in a confocal microscope," in *Proc. Amer. Control Conf.*, 2009, pp. 1682-1687.
- [30] Z. Shen and S. B. Andersson, "Tracking multiple fluorescent particles in two dimensions in a confocal microscope," in *Proc. IEEE Conf. Decision Control*, 2009, pp. 6052-6057.
- [31] D. Y. Abramovitch, S. B. Andersson, L. Y. Pao, and G. Schitter, "A tutorial on the mechanisms, dynamics and control of atomic force microscopes," in *Proc. Amer. Control Conf.*, 2007, pp. 3488-3502.
- [32] J. E. Jonkman and E. H. K. Stelzer, "Resolution and Contrast in Confocal and Two-photon microscopy," in *Confocal and Two-Photon Microscopy. Foundations, Applications, and Advances*. New York: Wiley-Liss, 2002, ch. 5, pp. 101-125.
- [33] C. Kural, H. Balci, and P. R. Selvin, "Molecular motors one at a time: FIONA to the rescue," *J. Phys: Cond. Matt.*, vol. 27, no. 47, pp. S3979-S3995, 2005.
- [34] S. B. Andersson and T. Sun, "Linear optimal control for tracking a single fluorescent particle in a confocal microscope," *Appl. Phys. B*, vol. 94, no. 3, pp. 403-409, 2009.
- [35] *Applied Optimal Control*. San Francisco, CA: Taylor and Francis, 1975.
- [36] M. J. Saxton and K. Jacobson, "Single-particle tracking: Applications to membrane dynamics," *Ann. Rev. Biophys. Biomol. Struct.*, vol. 26, pp. 373-399, Jun. 1997.
- [37] A. J. Berglund and H. Mabuchi, "Performance bounds on single-particle tracking by fluorescence modulation," *Appl. Phys. B*, vol. 83, no. 1, pp. 127-133, Apr. 2006.
- [38] A. J. Berglund, K. McHale, and H. Mabuchi, "Fluctuations in closed-loop fluorescent particle tracking," *Opt. Expr.*, vol. 15, no. 12, pp. 7752-7773, Jun. 2007.
- [39] A. J. Berglund, K. McHale, and H. Mabuchi, "Feedback localization of freely diffusing fluorescent particles near the optical shot-noise limit," *Opt. Lett.*, vol. 32, no. 2, pp. 145-147, Jan. 2006.
- [40] D. Thomann, D. R. Rines, P. K. Sorger, and G. Danuser, "Automatic fluorescent tag detection in 3D with super-resolution: Application to the analysis of chromosome movement," *J. Microscopy*, vol. 208, no. 1, pp. 49-64, Oct. 2002.
- [41] K. Kis-Petikova and E. Gratton, "Distance measurement by circular scanning of the excitation beam in the two-photon microscope," *Microscopy Res. Tech.*, vol. 63, no. 1, pp. 34-49, Jan. 2004.
- [42] D. Y. Abramovitch, S. Hoen, and R. Workman, "Semi-automatic tuning of PID gains for atomic force microscopes," in *Proc. Amer. Control Conf.*, 2008, pp. 2684-2689.
- [43] A. Sebastian and S. M. Salapaka, "Design methodologies for robust nano-positioning," *IEEE Trans. Control Syst. Technol.*, vol. 13, no. 6, pp. 868-876, Nov. 2005.